Improving the Functionality and Performance of AA2024 Corrosion Sensing Coatings with Nanocontainers

Tiago L.P. Galvão, Isabel Sousa, Manon Wilhelm, Jorge Carneiro, Jakub Opršal, Helena Kukačková, Vladimír Špaček, Frederico Maia, José R.B. Gomes, João Tedim, Mário G.S. Ferreira

PII: S1385-8947(18)30263-8
DOI: https://doi.org/10.1016/j.cej.2018.02.061
Reference: CEJ 18540

To appear in: *Chemical Engineering Journal*

Received Date: 21 November 2017
Revised Date: 7 February 2018
Accepted Date: 12 February 2018

Please cite this article as: T.L.P. Galvão, I. Sousa, M. Wilhelm, J. Carneiro, J. Opršal, H. Kukačková, V. Špaček, F. Maia, J.R.B. Gomes, J. Tedim, M.G.S. Ferreira, Improving the Functionality and Performance of AA2024 Corrosion Sensing Coatings with Nanocontainers, *Chemical Engineering Journal* (2018), doi: https://doi.org/10.1016/j.cej.2018.02.061

Improving the Functionality and Performance of AA2024 Corrosion Sensing Coatings with Nanocontainers

Tiago L. P. Galvão[a,*], Isabel Sousa[a], Manon Wilhelm[a], Jorge Carneiro[a], Jakub Opršal[b], Helena Kukačková[b], Vladimír Špaček[b], Frederico Maia[c], José R. B. Gomes[d], João Tedim[a,*], Mário G. S. Ferreira[a]

[a] *CICECO-Aveiro Institute of Materials, Department of Materials and Ceramic Engineering, University of Aveiro, 3810-193 Aveiro, Portugal*

[b] *SYNPO, S. K. Neumanna 1316, 532 07 Pardubice, Czech Republic*

[c] *Smallmatek, Small Materials and Technologies, Rua dos Canhas, 3810-075 Aveiro, Portugal*

[d] *CICECO-Aveiro Institute of Materials, Department of Chemistry, University of Aveiro, 3810-193 Aveiro, Portugal*

*Corresponding author.

E-mail addresses: tlpgalvao@ua.pt (T. L. P. Galvão); joao.tedim@ua.pt (J. Tedim); Phone: +351938403485; +351961688838.

ABSTRACT

The compatibility between nanocontainers and coating formulations is perhaps the last frontier in the quest for functional coatings. Sensing coatings for early metallic corrosion detection is an urgently needed technology by aeronautical companies to mitigate the costs of corrosion through continuous monitoring. In this work, we revisit phenolphthalein encapsulated silica nanocapsules, which were incorporated into a water-based lacquer, resulting in a novel corrosion sensing coating for aluminum alloy 2024 with improved functionality and standard performance. The ability of the coatings to detect corrosion by color change was investigated by immersion and salt-spray tests. During these tests, it was clearly demonstrated that encapsulation of the active compound is essential to obtain a functional coating, since the shell of the silica nanocapsules minimizes the detrimental interaction of the active compound with the coating formulation. The compatibility between nanostructured additives and coatings is almost never taken into consideration in the literature. Herein this aspect evidences the positive effects of active agent encapsulation, which is explored in terms of reactivity, viscoelastic properties, curing, thermal stability, release and leaching studies, hardness, mechanical properties and corrosion resistance. Computer simulations based on the density functional theory and periodic structural models were performed to unveil the interaction mode of phenolphthalein with the metallic surface.

1. Introduction

It is critical for the aeronautical industry that the next generation of smart coatings allows the early detection and continuous monitoring of corrosion. Once corrosion is detected, preventive actions can be taken in order to mitigate its costs, such as restoration of the affected zone and partial substitution of the coating. The need to confer a corrosion sensing ability to coatings has demanded the efforts of researchers around the globe, including those working in large agencies such as NASA [1]. The present work addresses this demand by providing a market ready nanocontainer-based coating.

Traditional corrosion sensing technology usually involves complicated strategies, such as electrochemical sensors [2], sub-surface image techniques [3], scanning electrochemical microscopy [4], optical microring resonation [5] or electrically conductive paints together with printed wiring for the wireless transmission of the results [6].

An early simpler technology [7] to obtain coatings equipped with intrinsic corrosion sensing ability was the direct dispersion of pH sensors in coating formulations [8]. The rationale behind this strategy is that once corrosion ensues, this leads to localized effects in metals [9] with an acidic pH in anodic regions and an alkaline pH in cathodic regions [10]. However, in the case of corrosion inhibitors, the direct interaction between the inhibitors and coating formulations, despite enhancing active corrosion protection, could deteriorate the coatings barrier properties, which leads to the proliferation of corrosion processes [11]. With this in mind, and in order to minimize the interaction between pH sensors and coating formulations, Maia *et al.* developed nano [12] and microcontainers [13] for the encapsulation of pH sensors and demonstrated the concept of nanocontainer-based sensing coatings. Revisiting phenolphthalein encapsulated silica nanocapsules (SiNC-PhPh) [12] in the present work, a surface engineering research group joins forces with a nanocontainers' producing

startup and a coating manufacture company to produce a corrosion sensing coating (Figure 1) with improved functionality for one of the most common alloys used in the aeronautical industry: the aluminum alloy 2024 (AA2024). The coating system developed in this work has several main advantages concerning the current state of the art of sensing coatings: i) regarding sensing coatings resulting from the direct dispersion of functional organic compounds on polymeric matrices [7,8], the use of SINC to encapsulate pH sensors avoids the direct and detrimental interaction of organic compounds with the coating [11], resulting, as demonstrated in the presented work, in a new coating with comparatively better performance in terms of corrosion protection, which is fundamental for end users in the aeronautical industry, while also improving its hardness and viscoelastic properties, increasing the thermal stability, and reducing the leaching of organic compounds under extreme pH conditions; ii) regarding sensing coatings which already make use of the encapsulation of the sensing compound [12,13], the present coating has a unique combination of polymer matrix and nanocontainers that maintain an initial transparent coating (usually, to enhance the change of color other coatings employ an initial white color) and are already in the final upscaled form and currently existent in the market.

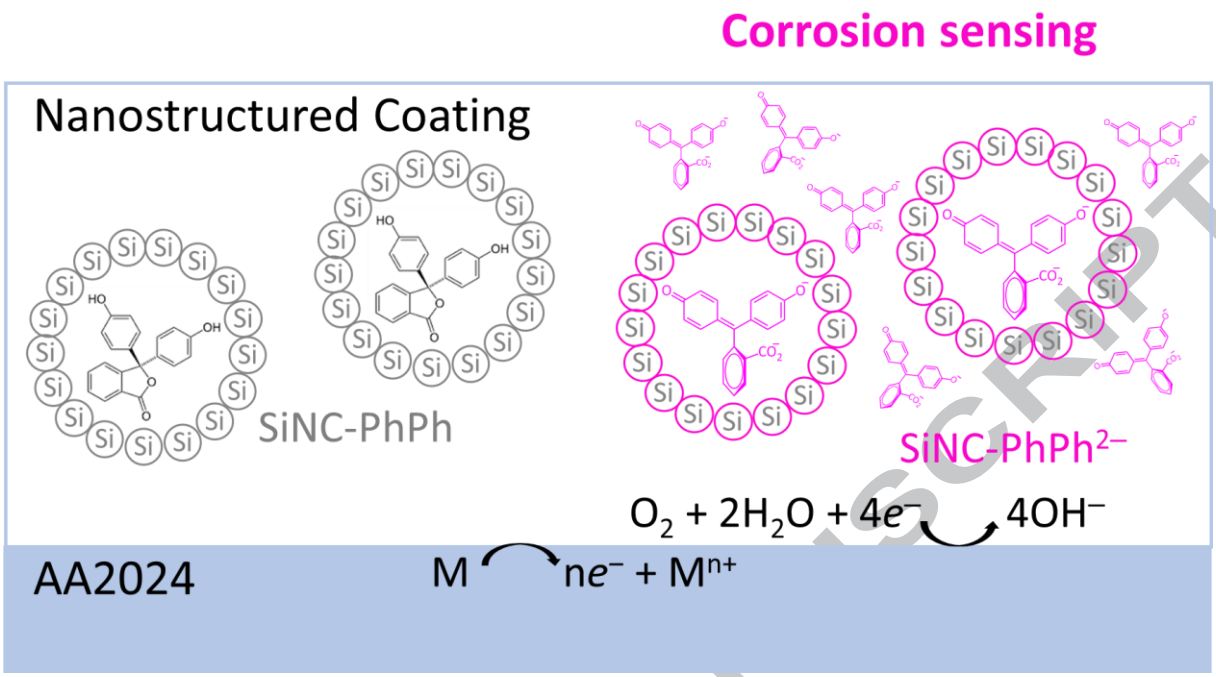

Figure 1. Corrosion sensing mechanism of a SiNC-PhPh corrosion sensing coating for AA2024.

The field of nanocontainer based functional coatings and of sensing coatings in particular, is still in its infancy. The compatibility between nanocontainers and polymeric coating formulations is a rarely addressed aspect, yet fundamental for the application of new functional coatings in the real world. After incorporation of nanocontainers into coating formulations, besides acquiring new functionalities, coatings should be able to maintain their original properties and perform according to standard tests required for industrial application. In the present work, SiNC-PhPh were incorporated into a water borne high-performance lacquer. For comparison, the same amount of PhPh that was encapsulated in the silica nanocontainers was also added directly to the coating. First, it was demonstrated that the direct addition of active agents into the coatings has limited applicability, since only the nanocontainer based coating responded adequately to the localized corrosion effects. Secondly, the new coating was submitted to rigorous standard performance tests demanded by the industry, through investigation of its rheology, leaching, curing, thermal stability,

hardness, mechanical properties and corrosion resistance. It was demonstrated that encapsulation of PhPh in SiNC keeps the original properties of the coating mostly intact, while providing corrosion sensing ability and increasing corrosion resistance.

Moreover, the drawbacks of directly adding active organic compounds to coating formulations are clearly shown in the present study, such as the 'deactivation' of the sensing compound in some formulations, lower responsive ability to surrounding conditions, and damaging interaction with the coating formulation resulting in a lower protection of the metal by barrier effect. These findings reinforce the importance of nanocontainers to achieve functional coatings.

2. Experimental section

2.1. Materials

Phenolphthalein (PhPh), cetyltrimethylammonium bromide (CTAB) (99 %), tetraethoxysilane (TEOS) (99.9 %), ammonia solution (NH_4OH) (25–28 %), ethanol (95 %) and cyclohexane (99.5 %) were acquired from Sigma-Aldrich and used for the synthesis of SiNC-PhPh without any further purification.

2.2 Synthesis of SiNC-PhPh

SiNC-PhPh were produced by SMALLMATEK Lda. according to an upscaled procedure of an oil-in-water microemulsion described in a previous work [12], using a mixture of cyclohexane and ethanol (1.5:1) as the oil phase. The obtained precipitate was filtered, washed with distilled water and conserved as slurry for the application in coating formulations. 10 wt. % was considered to be the amount of encapsulated PhPh in SiNC,

according to a previous study [12]. Hence, this percentage was used in the calculation of the amount of PhPh to be dispersed directly in the formulation for comparison purposes.

2.3. Pre-treatment of aluminum substrates

Aluminum alloy 2024-T3 (AA2024) plates were washed with deionized water, followed by acetone for removal of dust and degreasing. Then, AA2024 plates were chemically etched following a three-step industrial cleaning procedure ("Aluminetch") consisting of: 1) alkaline treatment in Metaclean T2001 [(48 ± 2) g L^{-1}] at (65 ± 5) °C for 25 min; 2) alkaline etching in Turco Liquid Aluminetch N2 [(65 ± 5) g L^{-1}] at (60 ± 5) °C for 45 s; and 3) acid etching in a Turco Liquid Smutgo NC [(180 ± 10) ml L^{-1}] at (30 ± 5) °C for 7 min. After each step the metallic plates were thoroughly washed with distilled water, and, in the end, dried at room temperature.

2.4. Coating formulation

A water-soluble acrylic urethane emulsion produced by SYNPO, commercially available as LACQUER AQ CC 080, was used in this work. It was chosen since it combines top performance and high gloss with significantly lower and less toxic emissions of volatile organic compounds (VOC) than solvent-based formulations. The weight percentage of solids in the mixture was 35 wt. % and it was used in combination with hardener AQ BU 16 (SYNPO), in a 2.5 AQ CC 080 : 1 AQ BU 16 mixing ratio. After application of the coating formulation, the curing process was the following: 24 h at room temperature (≈ 23 ºC) followed by 1 h in an oven at 100 ºC.

AC alkyd Hydrospol D101 (D101, produced by Spolchemie) was also used in this work to extend our approach to other formulations. This formulation, which has a solids content of 44%, has the advantage of curing in air without the need of a curing agent. Nevertheless,

Additol VXW 4940 (produced by Allnex), a siccative to accelerate the curing, was added in low percentage (3 wt %) immediately before the deposition of the film and after the dispersion of the nanocapsules. After application, D101 was cured for 48 h at room temperature (≈ 23 ºC).

2.5. Mixing of SiNC-PhPh in the formulation and coating application

The dispersion of SiNC-PhPh in LACQUER AQ CC 080 was achieved using the following methodology: 1) pre-dispersion of the original SiNC-PhPh slurry in water for 24 h; 2) filtration of the product, guaranteeing that a sufficient amount of water is present to keep the capsules hydrated; 3) mixing of SiNC-PhPh with the main component of the formulation and magnetic stirring for another 24 h.

The investigated coatings in this work (Table 1) were the original formulation, LACQUER AQ CC 080 (080), and 080 with 3 % of dispersed SiNC-PhPh particles (080-SiNC-PhPh). For comparison, the active compound (PhPh) was also dispersed directly in the polymeric matrix in a proportion of 0.3 %, which corresponds to the encapsulated amount in the particles (referred hereafter as 080-PhPh).

In the case of D101, the dispersion of the particles (3 % SiNC-PhPh) was performed by ultrasound for 15 minutes.

The ratio of particles in the formulation is calculated considering the mass of dry particles to the mass of solids content in the formulation.

The coatings were applied using a gap film applicator with a slit of 150 μm, which resulted in a dry film thickness of (30 ± 2) μm.

Table 1. Description of the coating systems studied in this work.

System acronym	Description
080	LACQUER AQ CC 080
080-PhPh	LACQUER AQ CC 080 with 0.3 % PhPh
080-SiNC-PhPh	LACQUER AQ CC 080 with 3 % dispersed SiNC-PhPh particles
D101-SiNC-PhPh	AC Alkyd Hydrospol D101 with 3 % dispersed SiNC-PhPh particles

2.6. Standard tests and characterization

Immersion tests in 5 % NaCl and salt-spray tests according to the International Standard ISO 9227 were used to examine the coating functionality for corrosion detection of AA2024. In the case of the salt-spray tests, on a small section of each plate, an X scribe was made in order to accelerate corrosion and coatings response.

The rheological study of the formulations was performed using a Kinexus lab+ rotational rheometer, with a 4° cone geometry of 40 mm diameter and a gap of 150 µm, at T = 298 K. The viscosities were measured in rotational mode using a shear rate sweep between 0.1 and 1000.0 s^{-1}, while measuring 5 points per decade. The viscoelastic properties were obtained using a constant shear strain of 2 % and a frequency sweep from 0.1 to 10 Hz, sufficient to observe the crossover between the loss (viscous) modulus (G”) and the storage (elastic) modulus (G’), together with 10 points per decade. The shear strain corresponding to the linear viscoelastic region was chosen after performing an amplitude sweep with shear strains between 0.01 and 100 %.

The glass transition temperatures (T_g) of several cured coating formulations were measured in a TA Instruments Q2000 differential scanning calorimeter (DSC). The cured formulation samples, with and without particles, were sealed in aluminum crucibles and measured according to convention (ISO 11357-2).

The thermal stability of the coatings was studied by thermogravimetric analysis (TG/DTA), using a Setaram–Labsys system under air atmosphere, with a heating rate of 10 ºC min^{-1} from room temperature up to 200 ºC.

For the characterization of the reaction product between PhPh and isocyanates, size exclusion chromatography (SEC) was carried out using a Waters Alliance 2695 Separations Module with a Waters 2414 refractive index (RI) detector using two Agilent PLgel Mixed-E columns 300 × 7.5 mm. The mobile phase was tetrahydrofuran (THF) at a flow rate of 1 mL/min. The columns were calibrated by 10 polystyrene standards covering a molar mass range of 162 – 35,000 g/mol. The sample was injected as a 100 mL THF solution with a concentration of approximately 0.3 % w/v.

The FT-IR absorbance spectrum was measured using a Nicolet Impact 400D apparatus with the sample applied on a KRS-5 slide.

The release of PhPh from silica nanocapsules and leaching of PhPh from coatings were performed by means of UV-Vis spectroscopy using a Sarspec SPEC SPEED+ UV/Vis equipment with a quartz cuvette (l = 1 cm). Calibration curves at different conditions were performed and their correlation coefficient, from at least 5 standards, was higher than 0.9999.

For the release studies, a suspension of SiNC-PhPh (20 mg) was prepared in 20 mL of solvent (pH 4 buffer, pH 10 buffer and 0.05 M NaCl) and kept under a stirring speed of 500 rpm for 24 h. At different time periods (0–24 h), aliquots were taken from the suspension with a syringe and filtered through PTFE membrane filters (0.45 mm pore size) to remove the capsules. Dilutions were performed when needed. Simultaneously, a suspension of SiNC-PhPh in ethanol was left under stirring for 24 h in order to determine the total release of PhPh from silica capsules (determination of loading content).

Leaching studies were performed for 080-PhPh and 080-SiNC-PhPh using ~0.1000 g of free film in 10 mL solutions of 0.05 M NaCl, pH = 4, pH = 10 and pH = 11.5. The

solutions with the original 080 free film were used as the reference background. After each measurement, the aliquot was placed again in the immersion solution.

The hardness of the coatings was analyzed according to Martens microhardness (ISO 14577-1), while the influence of the particles on the mechanical properties of films was assessed by tensile testing according to ASTM D 1708. Films were prepared by application on a polypropylene substrate, to facilitate the removal of the coatings, and samples were cut out from the free film.

The corrosion protection performance of the coating systems for AA2024 in a 50 mM NaCl aqueous solution was evaluated by electrochemical impedance spectroscopy (EIS).

The measurements were carried out with a Gamry potentiostat/galvanostat/ZRA interface 1000 at open circuit potential with an applied 10 mV sinusoidal perturbation in the 100 kHz to 10 mHz frequency range, taking 7 points per decade. A conventional three electrode cell was used, composed of a saturated calomel reference electrode, a platinum foil as counter electrode, and the AA2024 substrates as the working electrodes, with a surface area of 3.35 cm^2. Measurements were performed 2 months after the preparation of the coated substrates.

3. Computational section

Density functional theory (DFT) calculations employing periodic structural models were performed here to understand the interaction of PhPh with two different aluminum surfaces and to aid the interpretation of EIS results. For comparison purposes, the interaction of 2-mercaptobenzothiazole (MBT) [14], an efficient corrosion inhibitor for aluminum alloys [15], with aluminum surface models was also considered.

The calculations were performed with the Quantum ESPRESSO (QE) suite of computer codes [16] and the Perdew–Burke–Ernzerhof (PBE) [17] exchange-correlation functional based on the generalized-gradient approximation of the DFT. The semi-empirical correction of Grimme (D2) was employed to take into account van der Waals interactions [18,19]. The nuclei and core electrons were described by ultrasoft pseudopotentials [20] available for PBE in the QE website (http://www.quantum-espresso.org/pseudopotentials/). The Kohn−Sham orbitals were expanded using planewave basis sets with 30 Ry cutoff for kinetic energy and 240 Ry cutoff for charge density. The first Brillouin Zone integrations were performed with the Gaussian smearing method using a smearing parameter of 0.02 and a 2 × 2 × 1 k-point mesh [21]. The optimization procedure was stopped after the forces acting on all atoms in a structure were lower than 10^{-3} Ry/au.

In order to understand the interaction of PhPh and MBT with the aluminum substrate, the adsorption energies of one molecule per supercell onto two aluminum surfaces, hydroxylated aluminum terminated α-Al_2O_3(0001) and Al(111), were analyzed. The two surfaces were chosen, since corrosion inhibitors may interact with the aluminum oxide layer formed on top of aluminum alloys [22–25], but also directly with the bare metal through defects on the oxide layer [22,23] and depending on the stability of the oxide layer under different pHs [24] and other electrolyte [25] conditions.

The α-Al_2O_3(0001) slab (Figure 2) consisted in an aluminum terminated model with 18 layers (Al O Al Al O Al Al O Al Al O Al Al O Al Al O Al). The model was described as a (2 × 2) hexagonal cell with a lattice parameter of a = 4.76 Å [26]. The slab was built from the bulk structure and all atomic positions were relaxed. After optimization of the structure, in the remaining calculations, the eleven bottom layers were kept frozen, while the upper seven were allowed to relax (Figure 2). Then, hydroxyl groups were added to the uppermost aluminum layer of the model until reaching a degree of hydroxylation of 75 %, i.e., 3 hydroxyl groups

per (2 × 2) supercell as suggested from the DFT studies in ref. [27], and as applied in a previous work [28].

The Al(111) surface slab models (Figure 2) were described as four (5 × 5) (111) layers (100 atoms) with an optimized lattice parameter of 4.060 Å [29], keeping frozen the two bottom layers of the slab, while the other two were relaxed.

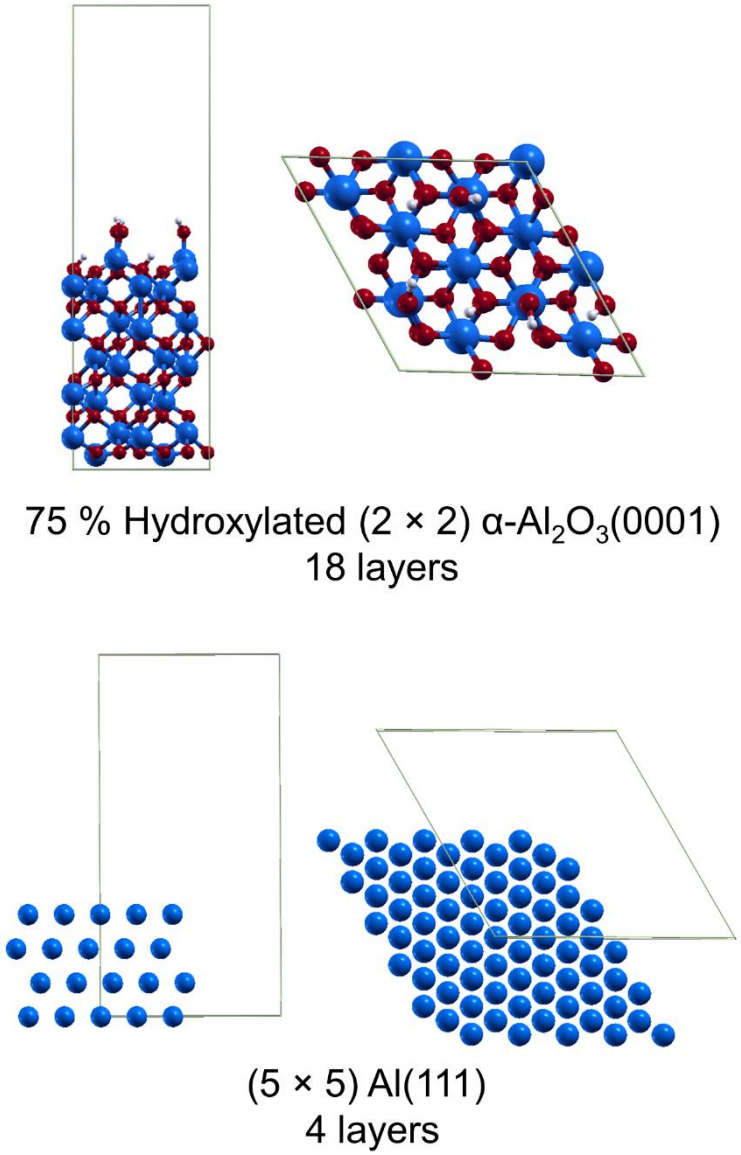

Figure 2. Representation of the supercells of the 75 % [27] hydroxylated aluminum terminated α-Al_2O_3(0001) model and the four layers (5 × 5) Al(111) model (spheres color code: Al - blue; O - red; H - white).

A vacuum region of at least 10 Å was kept between the top of the adsorbed molecule and the adjacent slab, and the artificial electric field perpendicular to the surface was corrected using the Bengtsson method [30].

The adsorption energies (E_{ads}) for PhPh and MBT onto the α-Al_2O_3(0001) and the Al(111) surface models were calculated as the difference of the total energy of the adsorbate@substrate systems and the sum of the total energies of the separated adsorbate and substrate fragments. Hence, negative values of the adsorption energy refer to stable adsorptions.

4. Results and discussion

4.1. Corrosion Sensing tests

Coated AA2024 plates were immersed in a 5 % NaCl solution in order to accelerate corrosion and verify if the coatings were able to detect the associated local change of pH [9,10]. A coated sample containing SiNC-PhPh (3 %) was compared with a coated sample prepared with directly dispersed PhPh with an amount corresponding to the active compound encapsulated in the nanocontainers (0.3 %) [12]. The need to encapsulate the pH indicator to obtain a sensing coating is demonstrated by the fact that only the sample with encapsulated PhPh (080-SiNC-PhPh) was able to change color and indicate the corrosion process (Figure 3).

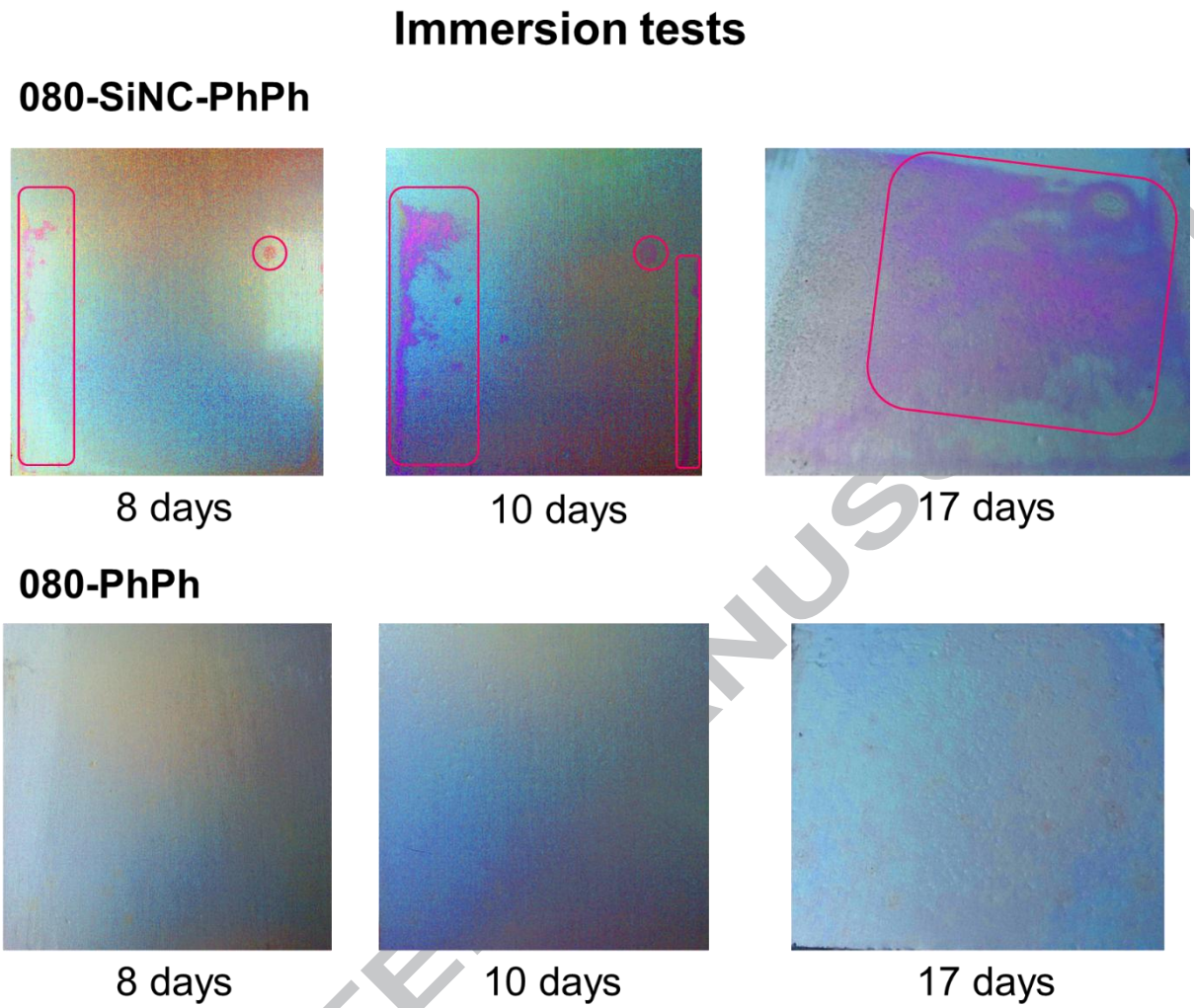

Figure 3. Immersion tests of coated AA2024 plates in 5 % NaCl. For clarity purposes, the color saturation of the all images was increased by the same amount.

It is possible to verify that the coating containing SiNC-PhPh starts to indicate the presence of corrosion, by the appearance of pink color, only after 8 days of immersion and before the corrosion process is even visible to the naked eye

In the case of 080-PhPh, after 8 days of immersion, several spots appear on the surface due to corrosion underneath, but no pink color is noticeable.

Standard near neutral salt-spray tests were also performed to analyze coatings response to accelerated corrosion conditions. A scribe was done in order to analyze their response to the accelerated corrosion process that occurs underneath. Again, only 080-SiNC-PhPh was

able to change color (and solely after two days of immersion) and indicate the corrosion process in the scribed zone (Figure 4). In Figure 4, is possible to verify that the addition of PhPh and SiNC-PhPh maintains the transparency of the original coating.

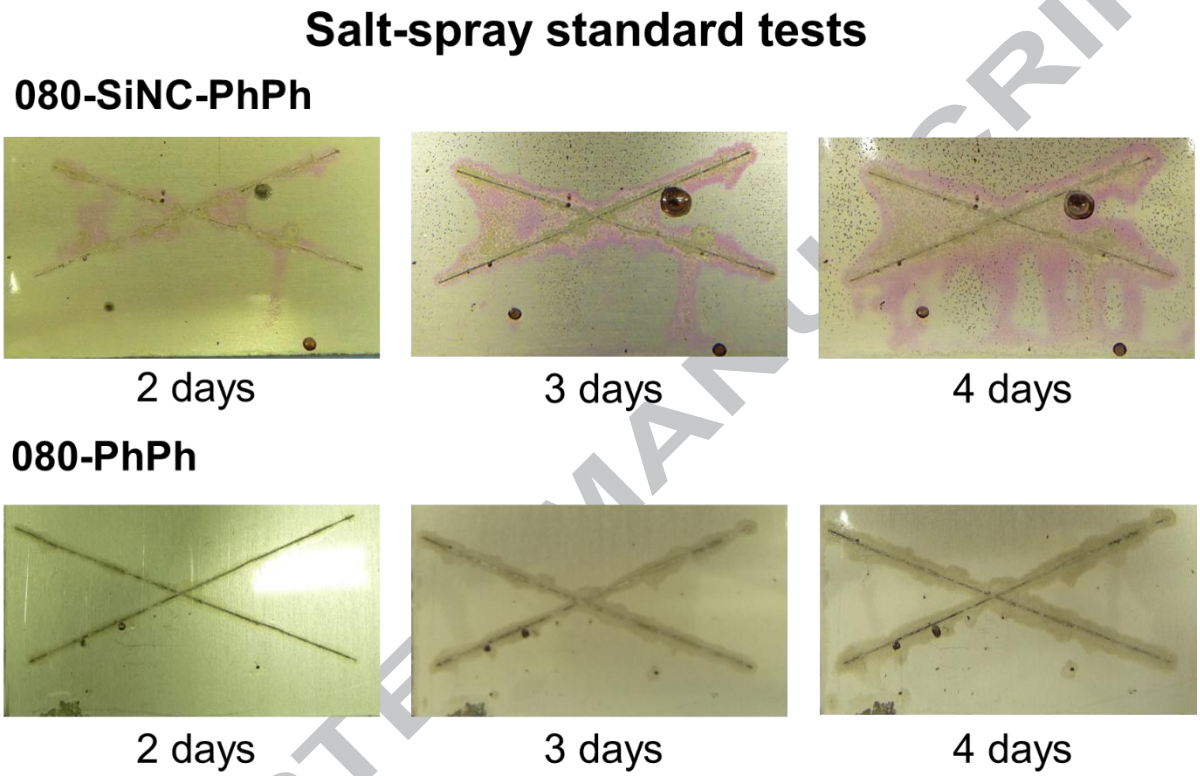

Figure 4. Standard neutral salt-spray tests of coated AA2024 plates with 080-SiNC-PhPh-3% and 080-PhPh-0.3% in 5 % NaCl.

The sample with free PhPh was never able to detect corrosion, which further supports the need to encapsulate pH indicators for the coatings to maintain sensing ability.

To ensure that the approach used herein can be extended to other polymeric formulations, SiNC-PhPh were also used, in this work, as sensing additives for D101. The results of near neutral salt-spray tests are presented in Figure 5, where a scribe was done to accelerate the corrosion process. D101-SiNC-PhPh is able to indicate corrosion after only four days of testing, and before corrosion is spotted. The functionality results of the D101-SiNC-PhPh coating demonstrate that the use SiNC-PhPh is not limited to the 080 coating. As

a result, D101-SiNC-PhPh was only characterized by salt-spray and immersion standard tests, but its good performance regarding these tests (the fact that it is able to detect corrosion by the change to pink color, before it is visible on the surface) suggest that SiNC-PhPh keep intact the barrier properties of the coating, demonstrating that D101-SiNC-PhPh is also a promising solution to be applied for corrosion sensing.

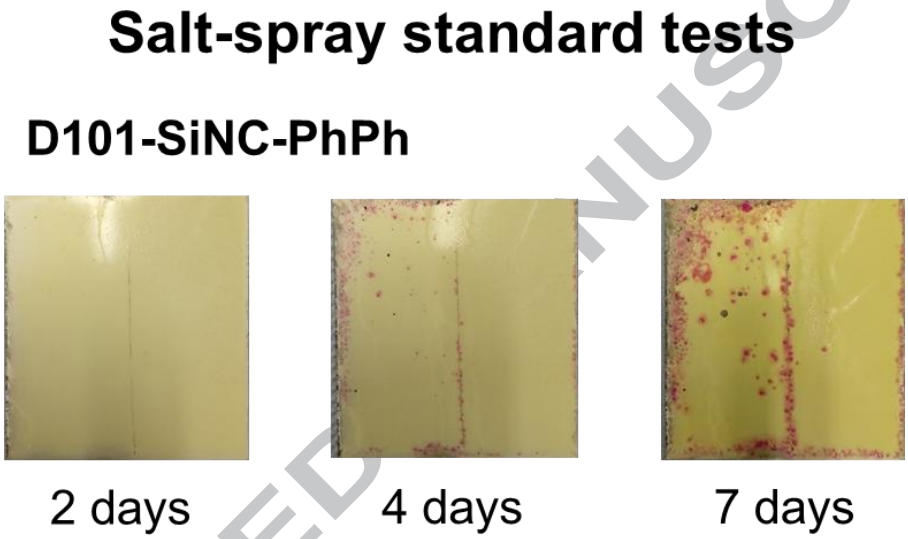

Figure 5. Standard neutral salt-spray tests of coated AA2024 plates with D101-SiNC-PhPh-3%.

The present combination of coating formulations and nanocontainers also present an improvement in terms of functionality for AA2024 over previous nanostructured sensing coatings [12,13].

4.2. Deactivation of PhPh

To analyze the effect on the visual signal of 080-PhPh, the amount of PhPh in the coating was increased from 0.3 % to 1 %. However, according to the results presented in Figure S1 of the Supplementary Material, the increase of the amount of PhPh in the formulation was not successful to enable corrosion detection. Hence, the reason for the lack of

signal in the case of directly added PhPh should be related to its interaction with the coating formulation.

AQ CC 080 coatings are obtained by mixing the main component of the formulation, a water-borne polyurethane emulsion, with a curing agent containing compounds with isocyanate groups to trigger the curing of the coating. These isocyanates are masked to be mixable with the binder without reacting with the water solvent. However, isocyanates can react with the hydroxyl groups present in the aromatic rings of PhPh to form urethanes, which might explain the deactivation of PhPh when added directly. To investigate this, an equimolar mixture of PhPh and isophorone diisocyanate was homogenized in tetrahydrofuran (THF) under dried atmosphere.

The reaction was monitored by FTIR (Figure 6). The spectra present an intense peak at ~2270 cm^{-1} corresponding to the isocyanate group (R–N=C=O). The solution was left to react in the presence of a catalyst (dibutyltin dilaurate). After 24 hours, the intensity of the isocyanate peak decreased to approximately two thirds of the initial peak, while several peaks associated with a urethane bond appear. This proves that the isocyanate groups react with PhPh.

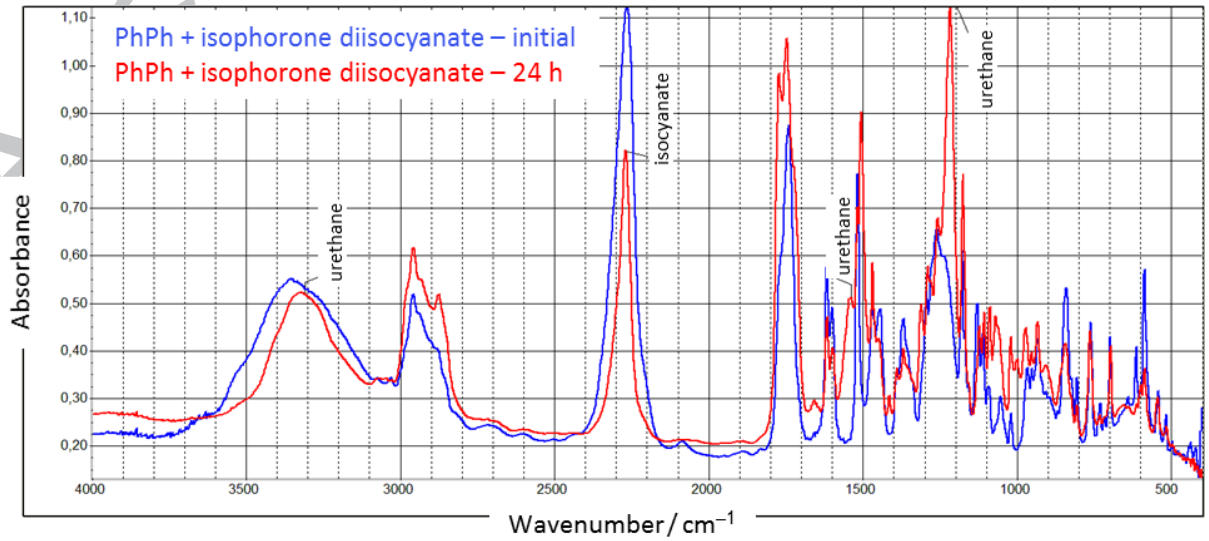

Figure 6. FTIR spectra of the PhPh and isophorone diisocyanate equimolar solution immediately after mixing (blue) and after 24 h (red).

After 5 days of reaction, the mixture was fully polymerized. The resulting white polyurethane was diluted again in THF to measure its molecular weight by size exclusion chromatography (SEC). An average molecular weight of 3839 g mol^{-1} was obtained, corresponding approximately to a chain with seven urethane units.

Additionally, a similar test was performed in order to investigate the compatibility of PhPh with the hardener of the 080 coating formulation (AQ BU 16). Results were compared with the ones obtained previously and similar conclusions can be drawn. A mixture of PhPh and hardener, with a ratio of approximately 1:1 regarding the functional groups, was homogenized in tetrahydrofuran (THF) under dried atmosphere. SEC measurements presented in Supplementary Material (Figures S3 and S4) were performed after 5 hours at 60 ºC and 7 days at room temperature. These results revealed the presence of high molecular weight peaks, consistent with a reaction between PhPh and the hardener.

In the case of PhPh encapsulated in SiNC, the active compound may be protected, by the silica shell, from reacting with isocyanate groups during the curing of the film. Hence, it would be available to provide a pink coloration indicating the change of pH during corrosion, unlike the free PhPh. While the reaction between the hydroxyl groups of PhPh and the isocyanate groups of the hardener may not be the sole factor explaining the deactivation of directly added PhPh, it is shown here to be a factor to consider. Moreover, this factor may not be limited to sensing coatings, since the encapsulation of organic compounds to limit their interaction with coating formulations is also relevant for corrosion protective coatings and antifouling coatings that rely on organic inhibitors [31] and organic biocides [32], respectively.

4.3. Rheology

A rheological study was performed (Figure 7) to understand the effect of additives on the viscosity and viscoelastic behavior of the main component of the formulation.

It is possible to verify that the addition of 0.3 % PhPh to the formulation keeps its viscosity almost intact, while the addition of 3 % SiNC-PhPh lowers it. Nevertheless, the resulting viscosity profile for 080-SiNC-PhPh is very similar to the original formulation, and the lowering of viscosity of only 5 mPa·s in the application range (1000 s^{-1}) is most likely due to the addition of water from the particles slurry. The lower viscosity of the formulation also supports the good dispersion of the particles, since large particles aggregates usually collide into each other when the formulation is forced to move, creating friction and increasing the viscosity. As it is evident by the remaining properties (hardness, mechanical and corrosion protection), the lower viscosity does not influence the application of the film.

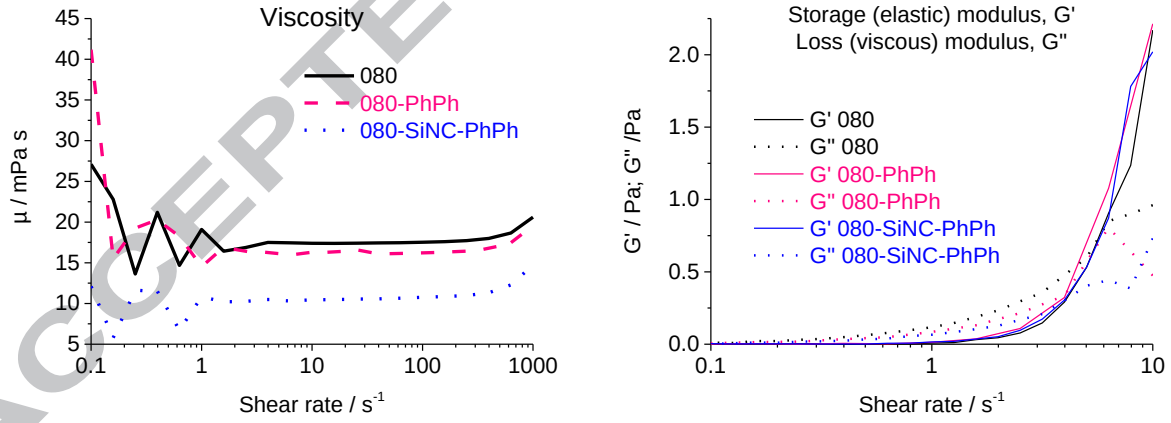

Figure 7. Rotational (left) and oscillatory (right) rheological properties of the 3 systems (original, with 0.3 % PhPh and with 3.0 % SiNC-PhPh).

The oscillatory rheological study shows a modulus pattern typical of viscoelastic liquids. For the three systems (080, 080-PhPh and 080-SiNC-PhPh), the loss modulus dominates ($G'' > G'$) at low frequencies (long timescales), implying a viscous behavior of the

formulation when it is stored. This explains the tendency of additives to sediment during storage, yet it was verified that mechanical stirring is sufficient for redispersion. Nevertheless, when comparing with the *G*'' value of the original formulation (080), the *G*'' value of 080-SiNC-PhPh is lower for low frequencies. This means that the addition of the capsules' slurry makes the formulation slightly less viscous dominated and slightly more stable during storage.

After a finite period, for high frequencies (fast processes), the formulation is elastically dominated (*G*' > *G*''), similar to the behavior of other inorganic additives [33], which is translated in a good levelling and sag behavior. The capsules help this behavior by increasing the difference between the two moduli, without drastically changing the timescale of the gel point (Table 2).

Table 2. **Rheological properties of the gel point.**

System	Frequency / Hz	Modulus / Pa
080	5.7	0.74
080-PhPh	4.1	0.36
080-SiNC-PhPh	3.9	0.29

4.4. Glass transition temperature and thermal stability

The glass transition temperature (T_g) is a critical parameter for coating performance. The coating glass transition reflects the thermal expansion when the coating goes from a hard glassy state to a rubbery state. Our coating has a T_g around 52 ºC (Table 3 and Figure S2 of the Supplementary Material) which is high enough to obtain a hard glassy state with favorable hardness and mechanical properties at room temperature, but low enough for the coating to cure without the need of higher temperatures that are inconvenient for large scale industrial applications.

With the addition of the nanocontainers, as well as the directly dispersed PhPh, the T_g is kept at temperature values ideal for the same type of applications of the original lacquer. It can be noticed that even though PhPh reacts with the 080's hardener, the T_g is kept nearly unchanged in the case of 080-PhPh. This can be because, when preparing a coating, the given proportion of curing agent is always calculated to be slightly in excess, in order for part of the isocyanates to react, if necessary, with any water present. This excess of curing agent may be enough to react with the directly added PhPh present in the formulation in a low percentage (0.3 %), resulting in the deactivation of PhPh (Sub-section 4.2. Deactivation of PhPh), but, at the same time, also enough to properly react with the main component of formulation maintaining the T_g unchanged. In the case of 080-SiNC-PhPh, the T_g is only slightly higher than the original formulation. This is in agreement with other studies where the addition of silica nanoparticles can modify the mechanical properties of the coatings, but leave T_g nearly unaffected [34]. Nevertheless, a second glass transition at higher temperatures was also detected, which is consistent with other works [35] and can be due to the formation of a second phase of polymeric structures around the SiNC.

Table 3. Glass transition temperatures measured by DSC.

System	T_g / ºC
080	51.7 ± 1.0
080-PhPh	51.6 ± 1.0
080-SiNC-PhPh	52.4 ± 1.0

The thermal stability of the cured coatings was investigated by thermogravimetric measurements. It is possible to observe that the direct addition of PhPh, leads to a slight decrease of the coating thermal stability for temperatures between 40 ºC and 100 ºC. The reason for this difference is not straightforward and since the decrease is not significant this

aspect was not further explored in the present work. Nevertheless, the encapsulation of PhPh improves this situation, maintaining the thermal stability of the original coating up to temperatures around 100-120 ºC.

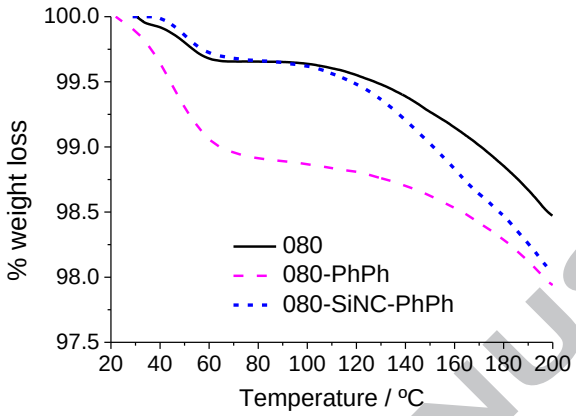

Figure 8. TG thermogram of the three coating systems (original, with 0.3 % PhPh and with 3.0 % SiNC-PhPh).

4.5. Release and leaching studies

The prepared SiNC-PhPh exhibit a spherical morphology, as can be noticed by the SEM results presented in Figure 9, with a size diameter between 300 and 450 nm. The response of SiNC-PhPh to pH in solution was investigated by measuring the release of PhPh under pH = 4, pH = 10 and NaCl 0.05 M (Figure 10). Under NaCl 0.05 M, the amount released was below the detection limit of the UV-Vis spectrophotometer, which indicates that SiNC do not release PhPh or the release is low enough to avoid leaching of PhPh, under near neutral accelerated corrosion conditions, when the nanocapsules are imbedded in a coating matrix. As it is possible to observe from the release profiles presented in Figure 10, there is a very small release of PhPh from SiNC at pH = 4. After 24 h, the release reaches 8.5 % of the total amount of encapsulated PhPh. Regarding the release at pH = 10, there is an increase in the amount released, reaching ~35 % after 1 h. At 24 h, there was no increase of the release of PhPh from SiNC. Despite the indicated value at 24 h being lower than at 1 h, this should be

due to reasons (readsorption of PhPh on the surface of the particles or the acid-base equilibrium displacing with time towards the neutral form, known to have much lower solubility in water than the anionic form) which don't seem to influence the performance of SiNC-PhPh for corrosion sensing, and therefore it is possible to assume that the maximum amount of PhPh released at pH = 10 is the one indicated at 1 h, ~35%.

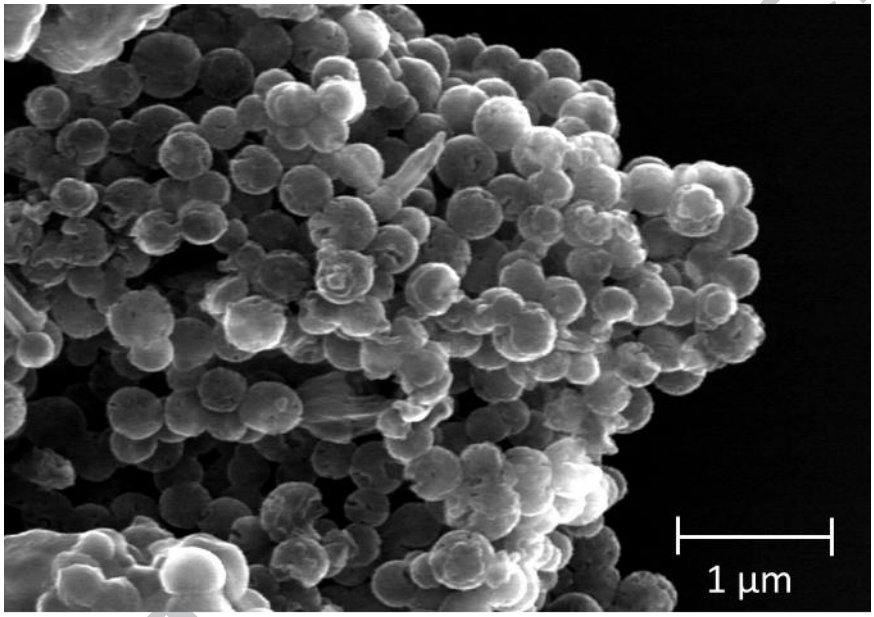

Figure 9. SEM image of SiNC-PhPh.

There are two main factors influencing the release of PhPh from SiNCs: the solubility of PhPh and the stability of SiNCs. At near neutral pHs, SiNCs are very stable, PhPh has very limited solubility and no release is noticed. Under acidic conditions (pH = 4), PhPh is released to the surrounding solution. The reason behind this is not exactly known, but should be related to the stability of SiNCs under acidic conditions (hydrolysis of non-hydrolyzed TEOS blocking some pores [36]) and/or higher solubility of PhPh under conditions of higher ionic strength (in the case of NaCl solutions, as the ionic strength increases, PhPh is also released more extensively [12]). At pH = 10, the surrounding solution is able to diffuse through the mesoporous shell of the nanocapsules, where some amount of PhPh already exists. After

reaching the core, where most of PhPh is present, the basic solution displaces the acid-base equilibrium of PhPh from the colorless neutral form to the pink anionic form, which is known to be more soluble and being able to diffuse to the surrounding solution.

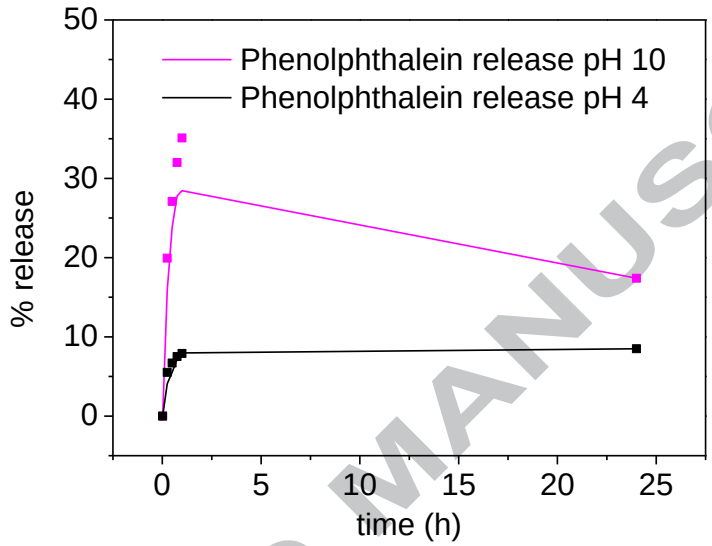

Figure 10. PhPh release profiles from SiNC at pH = 4 and pH = 10.

Following the release studies performed to analyze the sensitivity of SiNC to different conditions, leaching studies of free coating films (detached from a polypropylene substrate) in solution were also performed for 080-PhPh and 080-SiNC-PhPh under 0.05 M NaCl, pH = 4, pH = 10 and pH = 11.5 (Figure 11). Under near neutral accelerated corrosion conditions (NaCl 0.05 M), which are most likely to represent application conditions, no PhPh was detected after 15 days of exposure. Avoiding the leaching of active compounds during the working life of the coating is important not only from a coating functionality point of view, but also due to environmental concerns. Even for more aggressive conditions, the leaching of PhPh was not noticeable (pH = 4) or happened only in very minor percentages (pH = 10 and pH = 11.5) compared to the total amount that was added to the formulation (directly or encapsulated). Between directly adding PhPh or SiNC-PhPh, the only difference is that for pH

= 11.5, 080-PhPh leaches to a slightly greater extent than 080-SiNC-PhPh. Nevertheless, this release of active compound should only happen underneath the coating, in areas where hydroxide anions accumulate due to the onset of corrosion.

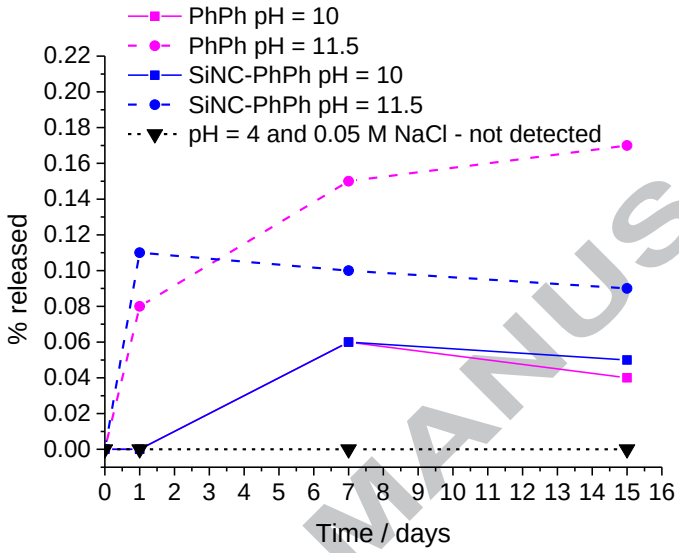

Figure 11. Leaching studies for 080-PhPh and 080-SiNC-PhPh free films.

During the immersion tests reported in Sub-section 4.1 (Corrosion Sensing Tests), in order to test if there was leaching of PhPh from the coatings (080-PhPh and 080-SiNC-PhPh) to the surrounding immersion solutions, aliquots of the immersion solution were collected after corrosion sensing was already triggered. The pH of the solution was increased to 10 by the addition of NaOH, but the solution remained colorless. This also indicates that the extent to which PhPh leaches to the surrounding 5 % NaCl solution, in the case of both samples, is below the concentration required to change the color of the solution and should be negligible.

4.6. Hardness and mechanical properties.

It is possible to verify that according to the Martens microhardness values presented in Table 4, 080-PhPh hardness values are in agreement with the original coating within the

standard deviation of the measurements. For 080-SiNC-PhPh the hardness values are slightly higher and reflect a higher resistance to scratching, which is in agreement with other studies that use silica nanoparticles as coating additives [37].

Concerning the mechanical properties (Table 4), the tensile strength of the three samples is nearly the same within experimental uncertainty, which means that the cohesive forces within the material are almost identical, regardless if 0.3 % PhPh or 3 % SiNC-PhPh are added to the original formulation.

Table 4. **Hardness and tensile tests results.**

Sample	Martens microhardness / $N \cdot mm^{-2}$	Tensile strength / MPa
080	132 ± 13	42.3 ± 3.6
080-PhPh	143 ± 1	37.5 ± 3.2
080-SiNC-PhPh	154 ± 3	37.9 ± 2.4

4.7. Corrosion resistance

The main objective of adding corrosion sensing additives to coatings is to provide them with sensing functionality, yet without compromising their barrier properties. Therefore, the corrosion resistance of coated AA2024 substrates under 0.05 M NaCl was evaluated by electrochemical impedance spectroscopy (EIS, Figure 12) for the three systems studied (080, 080-PhPh and 080-SiNC-PhPh).

According to EIS measurements over time (5 min, 1 day, 1 week and 2 months), for a frequency of 0.1 Hz, it is possible to obtain the following order of coating performance: 080-PhPh (worst) < 080 < 080-SiNC-PhPh (best).

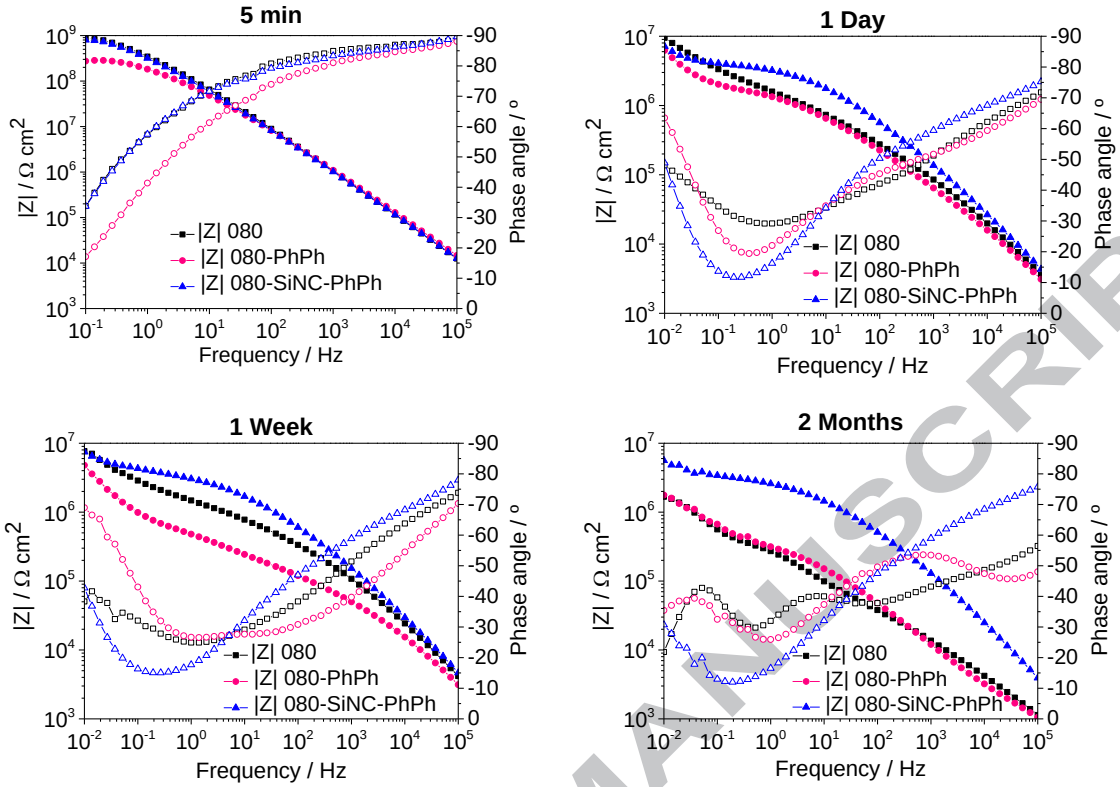

Figure 12. EIS results of the AA2024 coated substrates under 0.05 M NaCl.

Initially, the EIS spectrum obtained at 5 min for 080-SiNC-PhPh is very similar to the reference coating 080, across the whole frequency range. This supports that a good dispersion of the capsules in the coating was achieved, since any agglomeration would most likely have a detrimental impact in the initial barrier properties, by creating micro defects or other kind of pathways for the diffusion of electrolyte species. On the other hand, the direct addition of PhPh to the coating results in lower impedance at low frequencies, as can be seen in the spectrum obtained after 5 min, when compared to 080 and 080-SiNC-PhPh. Taking into account that only one time constant is detected at this stage (5 min) for all the three systems, the lower frequency plateau can be ascribed to resistive part of the coating response, namely the pore resistance [38]. The negative effect of adding directly PhPh to the coating can be due to a detrimental influence of PhPh on the crosslinking between polymer molecules during the curing process because of their interaction with the hardener or even due to the insolubility of PhPh in water based formulations, which not only has a detrimental effect on the barrier

properties of the coating but also, as it is evident from the immersion and salt-spray tests, on its functionality.

However, after 1 day of immersion, the impedance values decrease and additional time constants can be detected at intermediate and low frequencies, which can be attributed to the response of the native oxide film (f~10^1 Hz) and electrochemical processes ongoing at the metallic substrate (10^{-2}<f<10^{-1} Hz). The time-constant associated with the coating response is still visible at high frequencies (f>10^4 Hz). Although the decrease in impedance magnitude occurs for all the three systems under investigation, the decrease is more significant for 080-PhPh and 080 systems. After one week under immersion in 0.05 M NaCl, it is possible to verify that the system with PhPh (080-PhPh) clearly exhibits the lowest impedance values. Although another time constant appears at low frequencies indicating corrosion reactions on the metallic subtract after 1 day and 1 week, no color change is visible during the test due to the accumulation of hydroxide anions under these conditions still not reaching a certain threshold. In the case of the system that is able to indicate corrosion, 080-SiNC-PhPh, the comparatively lower decrease in magnitude of impedance implies that these processes are still not significant enough in order for a substantial concentration of hydroxide anions to accumulate locally and reach a pH at least higher than the pKa of PhPh (pK_a = 9.3 [39]), but, more importantly, high enough to allow the change of color of PhPh to be significant (usually, pH around 10) and high enough to allow the diffusion of the hydroxide anions through the coating to be sufficient to reach the SiNC-PhPh also in high concentrations (according to the leaching studies presented in subsection 4.5, probably a pH between 10 and 11.5).

After 2 months, the magnitude of impedance of the original coating lowers to values similar to 080-PhPh. Contrastingly, the EIS spectrum acquired for 080-SiNC-PhPh after 2 months of immersion is still similar to the spectrum obtained after 1 day of immersion. These results are consistent with the pictures presented in Table 5. The improved corrosion resistance of 080-SiNC-PhPh in comparison with the original coating (080) is possibly related

by the filler effect of the SiNC [37], as it is also demonstrated by the enhanced hardness results presented above. Nevertheless, a more in depth analysis of the enhanced protection by SiNC has been analyzed before in a work from our research group dedicated specifically to corrosion protection employing different SiNCs ("empty" and with a corrosion inhibitor encapsulated; in solution and impregnated in a coating) [36].

Table 5. AA2024 coated substrates under 0.05 M NaCl analyzed by EIS.

080			
			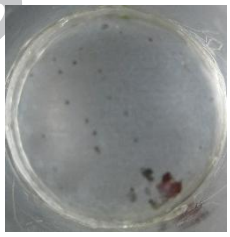
Initial	1 day	1 week	2 months
080-PhPh			
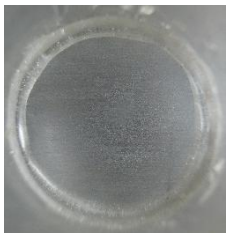	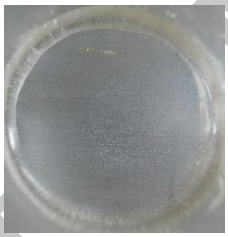	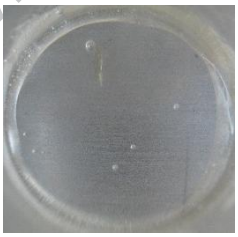	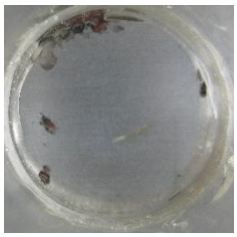
Initial	1 day	1 week	2 months
080-SiNC-PhPh			
	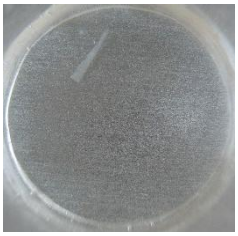	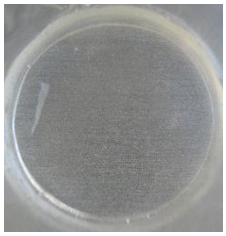	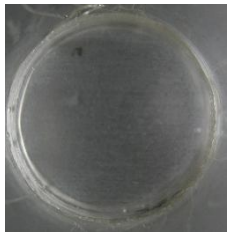
Initial	1 day	1 week	2 months

To understand why PhPh does not exhibit any noticeable active corrosion protection when present in the coating (080-PhPh) or after being locally released from the nanocontainers at high pHs during the corrosion process (080-SiNC-PhPh), periodic model DFT calculations were performed to obtain a qualitative picture of its interaction with the aluminum oxide layer, typically formed on top of AA2024 [22–25], and with the bare

aluminum surface, which is important to consider due to defects [22,23] and stability [24,25] of the oxide layer under different electrolyte conditions.

The adsorption energies for PhPh and MBT onto the Al_2O_3(0001) and Al(111) surface models presented in Figure 13 reveal that the interaction of PhPh with the bare aluminum surface is less favorable than in the case of MBT, a typical corrosion inhibitor for AA2024 [15] which presents active protective functionality when SiNC-MBT [36] are applied in coatings. PhPh adsorbs more favorably onto Al_2O_3(0001) than MBT [E_{ads}(PhPh@Al_2O_3(0001)) < E_{ads}(MBT@Al_2O_3(0001))], whereas MBT adsorbs more favorably onto Al(111) than PhPh [E_{ads}(PhPh@Al(111)) > E_{ads}(MBT@Al(111))]. This result indicates that it should be the adsorption onto the bare aluminum surface the fundamental interaction to understand the protection of the surface and achieve active corrosion protection functionality. Moreover, the more favorable interaction of potential corrosion inhibitors with Al(111) might be especially relevant when corrosion is onset and the stability of the oxide layer is lower. To understand the performance of organic corrosion inhibitors, several authors have pointed to the importance of the adsorption of the deprotonated form of the molecules [40–42], and the ability of functional groups to be ionized without being strong acids [43]. Indeed, PhPh has a less favorable adsorption energy than MBT when deprotonated on the surface (Figure 13), while its pK_a is significantly higher [pK_a(PhPh) = 9.3 [39], pK_a(MBT) = 7.0 [14]], resulting in a lower capacity of PhPh to adsorb onto aluminum surfaces [E_{ads}($PhPh_{deprot}$@Al(111)) > E_{ads}(MBT_{deprot}@Al(111))]. Costa *et al.*[44] have shown that an organic protective layer has an even greater insulating character than that of the oxide layer itself. Herein the simplest case of an organic protective layer was also investigated considering the adsorption of dimers with the molecules deprotonated on the surface. PhPh dimers have an adsorption energy less favorable than MBT dimers [E_{ads}(2$PhPh_{deprot}$@Al(111)) > E_{ads}(2MBT_{deprot}@Al(111))], while leaving more free aluminum atoms on the surface than MBT, making these atoms more available to interact with aggressive species. On the other

hand, MBT adopts a coordination more prone to insulate the aluminum surface and form a protective film than PhPh.

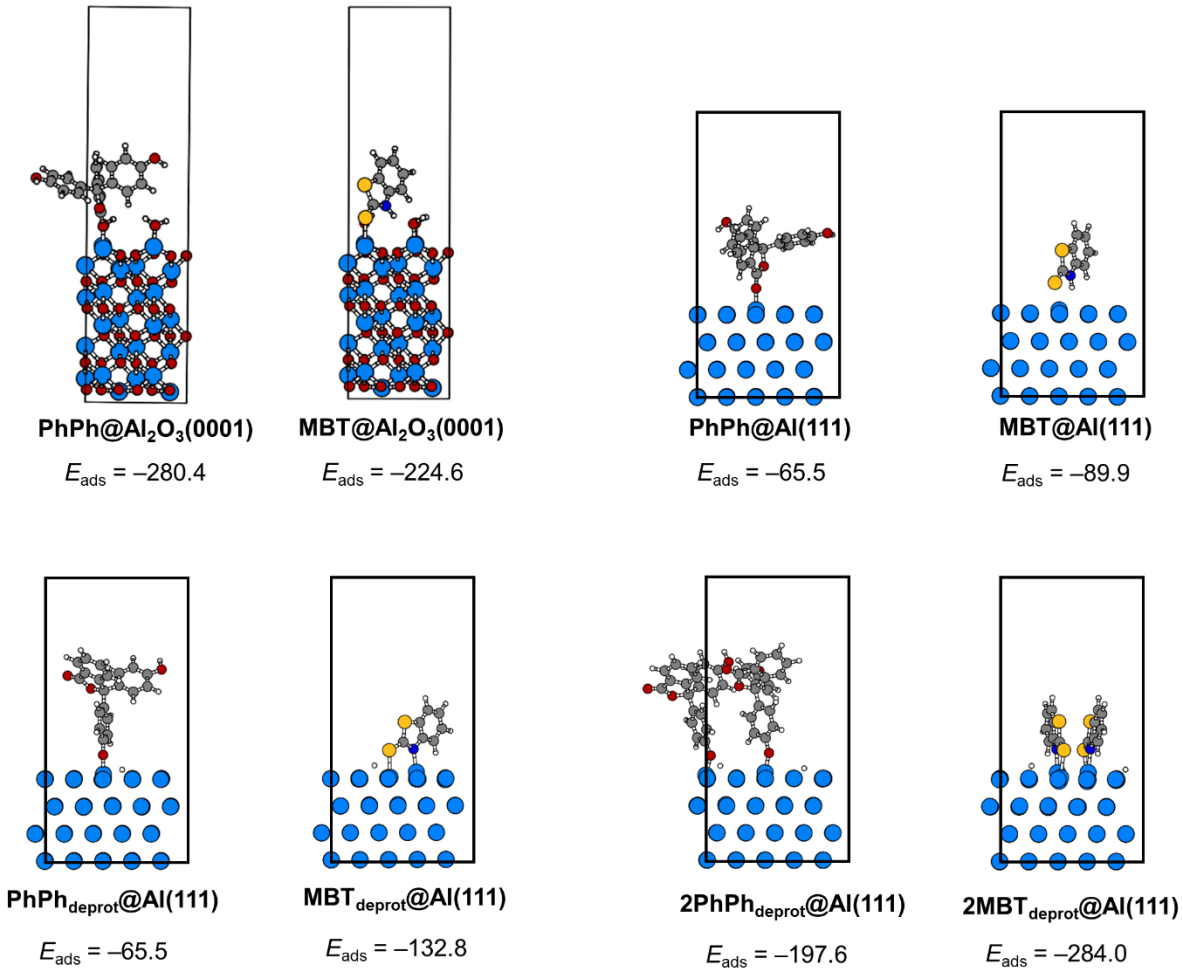

Figure 13. Preferential coordination modes for PhPh and MBT onto hydrogenated Al_2O_3(0001) and Al(111) surfaces and corresponding adsorption energies in $kJ \cdot mol^{-1}$.

5. Conclusions

A new coating formulation with improved functionality and performance is reported in this study. Phenolphthalein-encapsulated silica nanoparticles were used as an additive, and the properties of the obtained coating were compared with those attained when phenolphthalein is directly added to the formulation.

The following conclusions were obtained:

- Immersion and salt-spray tests of AA2024 coated plates containing SiNC-PhPh under 5 % NaCl solution proved functionality of the coatings for corrosion detection. Adding PhPh directly to the coating formulation was not effective indicating corrosion and its deactivation, due to detrimental interaction with the hardener, was demonstrated by FT-IR and GPC.
- Rheological studies revealed that the viscosity of the formulation, with addition of SiNC-PhPh, is consistent with a good dispersion of the particles while the slightly lower viscosity obtained is not detrimental for its application. The viscoelastic properties show that the addition of SiNC-PhPh might even help levelling and reduce sagging of the formulation.
- DSC measurements show that SiNC-PhPh maintain the glass transition temperature of the coating. The encapsulation of PhPh slightly improves the thermal stability of the coatings in comparison with directly added PhPh.
- Leaching studies do not show leaching of the active compound under normal application conditions.
- The addition of SiNC-PhPh improved the hardness and corrosion resistance of the coatings, maintaining its tensile strength.

These results are important to understand the advantages and disadvantages of using silica nanocapsules in functional coatings and lay the ground to build and improve a new line of coating products for corrosion sensing. Moreover, they seem transferable to self-healing [31] and anti-fouling coatings [32], where nanocontainers are also employed. This work also opens new objectives for the near future of corrosion sensing coatings, which is to quantify and directly correlate the change of color and its intensity with the level of degradation measured electrochemically.

Acknowledgements

This work was developed in the scope of the project CICECO – Aveiro Institute of Materials, POCI-01-0145-FEDER-007679 (Ref. FCT UID/CTM/50011/2013), financed by national funds through the FCT/MEC and when applicable co-financed by FEDER under the PT2020 Partnership Agreement. This work has received funding from the European Union's Horizon 2020 research and innovation programme under the Marie Skłodowska-Curie grant agreements No 645662. It was also financed in the framework of the project reference PTDC/QEQ-QFI/4719/2014, Project 3599 - Promover a Produção Científica e Desenvolvimento Tecnológico e a Constituição de Redes Temáticas (3599-PPCDT) and FEDER funds through COMPETE 2020, Programa Operacional Competitividade e Internacionalização (POCI). The authors also thank financial support from FCT and COMPETE (Programa Investigador FCT). JT thanks FCT for the research grant IF/00347/2013.

Appendix A. Supplementary data

Supplementary data associated with this article can be found, in the online version, at http://dx.doi.org/ .

References

[1] W. Li, L.M. Calle, Smart Coating for Corrosion Sensing and Protection, NASA Corros. Technol. Lab. https://corrosion.ksc.nasa.gov/SmartCoating.htm (accessed June 8, 2017).

[2] G.D. Davis, C.M. Dacres, Electrochemical sensors for evaluating corrosion and adhesion on painted metal structures, US5859537A, 1996.

[3] R.R. Alfano, P.-P. Ho, Sub-surface imaging under paints and coatings using early light spectroscopy, US6495833B1, 2000.

[4] H. Luo, C. Dong, S. Gao, C. Du, K. Xiao, X. Li, Sensing application in the precursor region of localized corrosion by scanning electrochemical microscopy, RSC Adv. 4 (2014) 56582–56595. doi:10.1039/C4RA01734J.

[5] R. Ahmed, A.A. Rifat, A.K. Yetisen, M.S. Salem, S.-H. Yun, H. Butt, Optical microring resonator based corrosion sensing, RSC Adv. 6 (2016) 56127–56133. doi:10.1039/C6RA11538A.

[6] Y. Kaneda, S. Ogawa, T. Sato, Corrosion detecting member and corrosion sensor, JP2007163324A, 2005.

[7] G.S. Frankel, R.G. Buchheit, J. Zhang, Corrosion-sensing composition and method of use, US20030068824 A1, 1999.

[8] A. Augustyniak, J. Tsavalas, W. Ming, Early Detection of Steel Corrosion via "Turn-On" Fluorescence in Smart Epoxy Coatings, ACS Appl. Mater. Interfaces. 1 (2009) 2618–2623. doi:10.1021/am900527s.

[9] F.J. Maile, T. Schauer, C.D. Eisenbach, Evaluation of corrosion and protection of coated metals with local ion concentration technique (LICT), Prog. Org. Coatings. 38 (2000) 111–116. doi:10.1016/S0300-9440(00)00080-1.

[10] A.C. Bastos, O. V. Karavai, M.L. Zheludkevich, K.A. Yasakau, M.G.S. Ferreira, Localised measurements of pH and dissolved oxygen as complements to SVET in the investigation of corrosion at defects in coated aluminum alloy, Electroanalysis. 22 (2010) 2009–2016. doi:10.1002/elan.201000076.

[11] D. Raps, T. Hack, J. Wehr, M.L. Zheludkevich, A.C. Bastos, M.G.S. Ferreira, O. Nuyken, Electrochemical study of inhibitor-containing organic–inorganic hybrid coatings on AA2024, Corros. Sci. 51 (2009) 1012–1021. doi:10.1016/j.corsci.2009.02.018.

[12] F. Maia, J. Tedim, A.C. Bastos, M.G.S. Ferreira, M.L. Zheludkevich, Nanocontainer-based corrosion sensing coating, Nanotechnology. 24 (2013) 415502. doi:10.1088/0957-4484/24/41/415502.

[13] F. Maia, J. Tedim, A.C. Bastos, M.G.S. Ferreira, M.L. Zheludkevich, Active sensing coating for early detection of corrosion processes, RSC Adv. 4 (2014) 17780. doi:10.1039/c4ra00826j.

[14] T.L.P. Galvão, A. Kuznetsova, J.R.B. Gomes, M.L. Zheludkevich, J. Tedim, M.G.S. Ferreira, A computational UV–Vis spectroscopic study of the chemical speciation of 2-mercaptobenzothiazole corrosion inhibitor in aqueous solution, Theor. Chem. Acc. 135 (2016) 78. doi:10.1007/s00214-016-1839-3.

[15] T.G. Harvey, S.G. Hardin, A.E. Hughes, T.H. Muster, P.A. White, T.A. Markley, P.A. Corrigan, J. Mardel, S.J. Garcia, J.M.C. Mol, A.M. Glenn, The effect of inhibitor structure on the corrosion of AA2024 and AA7075, Corros. Sci. 53 (2011) 2184–2190. doi:10.1016/j.corsci.2011.02.040.

[16] P. Giannozzi, S. Baroni, N. Bonini, M. Calandra, R. Car, C. Cavazzoni, Ceresoli, Davide, G.L. Chiarotti, M. Cococcioni, I. Dabo, A. Dal Corso, S. de Gironcoli, S. Fabris, G. Fratesi, R. Gebauer, U. Gerstmann, C. Gougoussis, A. Kokalj, M. Lazzeri, L. Martin-Samos, N. Marzari, F. Mauri, R. Mazzarello, S. Paolini, A. Pasquarello, L. Paulatto, C. Sbraccia, S. Scandolo, G. Sclauzero, A.P. Seitsonen, A. Smogunov, P. Umari, R.M. Wentzcovitch, QUANTUM ESPRESSO: a modular and open-source software project for quantum simulations of materials., J. Phys. Condens. Matter. 21 (2009) 395502. doi:10.1088/0953-8984/21/39/395502.

[17] J.P. Perdew, K. Burke, M. Ernzerhof, Generalized Gradient Approximation Made Simple, Phys. Rev. Lett. 77 (1996) 3865–3868. doi:10.1103/PhysRevLett.77.3865.

[18] S. Grimme, Semiempirical GGA-type density functional constructed with a long-range dispersion correction, J. Comput. Chem. 27 (2006) 1787–1799. doi:10.1002/jcc.20495.

[19] V. Barone, M. Casarin, D. Forrer, M. Pavone, M. Sambi, A. Vittadini, Role and effective treatment of dispersive forces in materials: Polyethylene and graphite crystals as test cases, J. Comput. Chem. 30 (2009) 934–939. doi:10.1002/jcc.21112.

[20] D. Vanderbilt, Soft self-consistent pseudopotentials in a generalized eigenvalue formalism, Phys. Rev. B. 41 (1990) 7892–7895. doi:10.1103/PhysRevB.41.7892.

[21] H.J. Monkhorst, J.D. Pack, Special points for Brillouin-zone integrations, Phys. Rev. B. 13 (1976) 5188–5192. doi:10.1103/PhysRevB.13.5188.

[22] G.E. Thompson, K. Shimizu, G.C. Wood, Observation of flaws in anodic films on aluminium, Nature. 286 (1980) 471–472. doi:10.1038/286471a0.

[23] C. Lanthony, J.M. Ducéré, M.D. Rouhani, A. Hemeryck, A. Estève, C. Rossi, On the early stage of aluminum oxidation: An extraction mechanism via oxygen cooperation, J. Chem. Phys. 137 (2012) 94707. doi:10.1063/1.4746943.

[24] A. Kolics, A.S. Besing, P. Baradlai, R. Haasch, A. Wieckowski, Effect of pH on Thickness and Ion Content of the Oxide Film on Aluminum in NaCl Media, J. Electrochem. Soc. 148 (2001) B251. doi:10.1149/1.1376118.

[25] S.Y. Yu, W.E. O'Grady, D.E. Ramaker, P.M. Natishan, Chloride Ingress into Aluminum Prior to Pitting Corrosion An Investigation by XANES and XPS, J. Electrochem. Soc. 147 (2000) 2952. doi:10.1149/1.1393630.

[26] M. Schreyer, L. Guo, S. Thirunahari, F. Gao, M. Garland, Simultaneous determination of several crystal structures from powder mixtures: the combination of powder X-ray diffraction, band-target entropy minimization and Rietveld methods, J. Appl. Crystallogr. 47 (2014) 659–667. doi:10.1107/S1600576714003379.

[27] C. Rohmann, J.B. Metson, H. Idriss, A DFT study on carbon monoxide adsorption onto hydroxylated α-Al_2O_3(0001) surfaces., Phys. Chem. Chem. Phys. 16 (2014) 14287–97. doi:10.1039/c4cp01373e.

[28] T.L.P. Galvão, C.S. Neves, M.L. Zheludkevich, J.R.B. Gomes, J. Tedim, M.G.S. Ferreira, How Density Functional Theory Surface Energies May Explain the Morphology of Particles, Nanosheets, and Conversion Films Based on Layered Double Hydroxides, J. Phys. Chem. C. 121 (2017) 2211–2220. doi:10.1021/acs.jpcc.6b10860.

[29] N. Kovačević, A. Kokalj, DFT study of interaction of azoles with Cu(111) and Al(111) surfaces: Role of azole nitrogen atoms and dipole-dipole interactions, J. Phys. Chem. C. 115 (2011) 24189–24197. doi:10.1021/jp207076w.

[30] L. Bengtsson, Dipole correction for surface supercell calculations, Phys. Rev. B. 59 (1999) 12301–12304. doi:10.1103/PhysRevB.59.12301.

[31] J. Tedim, S.K. Poznyak, A. Kuznetsova, D. Raps, T. Hack, M.L. Zheludkevich, M.G.S. Ferreira, , Enhancement of Active Corrosion Protection via Combination of Inhibitor-Loaded Nanocontainers, ACS Appl. Mater. Interfaces. 2 (2010) 1528–1535. doi:10.1021/am100174t.

[32] F. Maia, A.P. Silva, S. Fernandes, A. Cunha, A. Almeida, J. Tedim, M.L. Zheludkevich, M.G.S. Ferreira, Incorporation of biocides in nanocapsules for protective coatings used in maritime applications, Chem. Eng. J. 270 (2015) 150–157. doi:10.1016/j.cej.2015.01.076.

[33] P. Fu, K. Xu, H. Song, G. Chen, J. Yang, Y. Niu, R. Jerome, P. Dubois, H. Choi, J.R. Heath, Preparation, stability and rheology of polyacrylamide/pristine layered double hydroxide nanocomposites, J. Mater. Chem. 20 (2010) 3869. doi:10.1039/b927391c.

[34] S. Sprenger, Epoxy resins modified with elastomers and surface-modified silica nanoparticles, Polymer (Guildf). 54 (2013) 4790–4797. doi:10.1016/j.polymer.2013.06.011.

[35] I.A. Rahman, V. Padavettan, Synthesis of Silica Nanoparticles by Sol-Gel: Size-Dependent Properties, Surface Modification, and Applications in Silica-Polymer Nanocomposites—A Review, J. Nanomater. 2012 (2012) 1–15. doi:10.1155/2012/132424.

[36] F. Maia, J. Tedim, A.D. Lisenkov, A.N. Salak, M.L. Zheludkevich, M.G.S. Ferreira, Silica nanocontainers for active corrosion protection, Nanoscale. 4 (2012) 1287. doi:10.1039/c2nr11536k.

[37] Z. Luo, R.Y. Hong, H.D. Xie, W.G. Feng, One-step synthesis of functional silica nanoparticles for reinforcement of polyurethane coatings, Powder Technol. 218 (2012) 23–30. doi:10.1016/j.powtec.2011.11.023.

[38] M.L. Zheludkevich, R. Serra, M.F. Montemor, K.A. Yasakau, I.M.M. Salvado, M.G.S. Ferreira, Nanostructured sol–gel coatings doped with cerium nitrate as pre-treatments for AA2024-T3, Electrochim. Acta. 51 (2005) 208–217. doi:10.1016/j.electacta.2005.04.021.

[39] Q. Zhao, H. Wang, H. Zheng, Z. Sun, W. Shi, S. Wang, X. Wang, Z. Jiang, Acid–base bifunctional HPA nanocatalysts promoting heterogeneous transesterification and esterification reactions, Catal. Sci. Technol. 3 (2013) 2204. doi:10.1039/c3cy20868k.

[40] A. Kokalj, S. Peljhan, M. Finšgar, I. Milošev, What Determines the Inhibition Effectiveness of ATA, BTAH, and BTAOH Corrosion Inhibitors on Copper?, J. Am. Chem. Soc. 132 (2010) 16657–16668. doi:10.1021/ja107704y.

[41] A. Kokalj, S. Peljhan, J. Koller, The Effect of Surface Geometry of Copper on Dehydrogenation of Benzotriazole. Part II, J. Phys. Chem. C. 118 (2014) 944–954. doi:10.1021/jp409719c.

[42] S.U. Ofoegbu, T.L.P. Galvão, J.R.B. Gomes, J. Tedim, H.I.S. Nogueira, M.G.S. Ferreira, M.L. Zheludkevich, Corrosion inhibition of copper in aqueous chloride solution by 1H-1,2,3-triazole and 1,2,4-triazole and their combinations: electrochemical, Raman and theoretical studies, Phys. Chem. Chem. Phys. 19 (2017) 6113–6129. doi:10.1039/C7CP00241F.

[43] D.A. Winkler, M. Breedon, a. E. Hughes, F.R. Burden, A.S. Barnard, T.G. Harvey, I. Cole, Towards chromate-free corrosion inhibitors: structure–property models for organic alternatives, Green Chem. 16 (2014) 3349. doi:10.1039/c3gc42540a.

[44] D. Costa, T. Ribeiro, P. Cornette, P. Marcus, DFT Modeling of Corrosion Inhibition by Organic Molecules: Carboxylates as Inhibitors of Aluminum Corrosion, J. Phys. Chem. C. 120 (2016) 28607–28616. doi:10.1021/acs.jpcc.6b09578.

Highlights

- Nanocontainer based sensing coating for early AA2024 corrosion detection.
- Water based lacquer with phenolphthalein encapsulated silica nanocapsules.
- Encapsulation of active substances is benefic for functional coatings.
- Improved compatibility between nanostructured additives and coating formulation.
- The new formulation has passed standard tests necessary for industrial application.

Graphical abstract